

## Original Investigation

# Fluorescence Adaptive Optics Scanning Laser Ophthalmoscope for Detection of Reduced Cones and Hypoautofluorescent Spots in Fundus Albipunctatus

Hongxin Song, PhD; Lisa Latchney, MS; David Williams, PhD; Mina Chung, MD

 Supplemental content at [jamaophthology.com](http://jamaophthology.com)

**IMPORTANCE** Fundus albipunctatus (FA) is a form of congenital stationary night blindness characterized by yellow-white spots, which were classically described as subretinal. Although night blindness and delayed dark adaptation are hallmarks of this condition, recent studies have described a macular phenotype, particularly among older patients. Using a fluorescence adaptive optics scanning laser ophthalmoscope (FAOSLO), this study provides in vivo morphologic data at the cellular level in FA.

**OBJECTIVE** To study the cone photoreceptors and the albipunctate spots in FA at single-cell resolution.

**DESIGN, SETTING, AND PARTICIPANT** A woman in her 30s with FA underwent a complete ophthalmic examination, including conventional imaging tests, at the University of Rochester. A FAOSLO was used to obtain infrared reflectance images of the cone mosaic at the central fovea and along the superior and temporal meridians to 10° eccentricity. Cone density was measured at the foveal center, and cone spacing was calculated in sampling windows eccentrically. In the area of the albipunctate spots, autofluorescence FAOSLO images (excitation, 561 nm; emission, 624 Δ 40 nm) were simultaneously obtained.

**MAIN OUTCOMES AND MEASURES** Structural appearance of cones, cone density and spacing, and reflectance and autofluorescence of albipunctate spots.

**RESULTS** Cone density was reduced to 70% of the lower limit of the normal range at the foveal center ( $78.7 \times 10^3$  cones/mm<sup>2</sup>; mean [SD] reference range,  $199 [87] \times 10^3$  cones/mm<sup>2</sup>), and cone spacing was increased eccentrically to 10° (sign test,  $P = .045$ ). Individual cone central core reflectances appeared dim, suggesting loss of photoreceptor outer segments. The albipunctate spots were hypoautofluorescent. No photoreceptors or retinal pigment epithelium cells were identified at the locations of the albipunctate spots.

**CONCLUSIONS AND RELEVANCE** Although the predominant clinical symptom of night blindness and the electroretinography results suggest a primary rod dysfunction, examination with a FAOSLO demonstrates that cone density is also reduced. This finding may represent an early sign of progression to macular phenotype in FA. The hypoautofluorescence suggests that the albipunctate spots do not represent lipofuscin.

*JAMA Ophthalmol.* doi:10.1001/jamaophthol.2014.1079  
Published online June 12, 2014.

**Author Affiliations:** Center for Visual Science, University of Rochester, Rochester, New York (Song, Williams, Chung); Flaum Eye Institute, University of Rochester, Rochester, New York (Latchney, Chung); The Institute of Optics, University of Rochester, Rochester, New York (Williams).

**Corresponding Author:** Mina Chung, MD, Flaum Eye Institute, 601 Elmwood Ave, Box 659, University of Rochester, Rochester, NY 14642 ([mina\\_chung@urmc.rochester.edu](mailto:mina_chung@urmc.rochester.edu)).

**F**undus albipunctatus (FA) is a form of congenital stationary night blindness characterized by the presence of myriad discrete, small, round or elliptical yellow-white lesions, which have been clinically described as at the level of the retinal pigment epithelium (RPE).<sup>1</sup> Disease-causing mutations of the *RDH5* (OMIM 601617) gene have been identified in patients with FA.<sup>2,3</sup> The *RDH5* gene encodes 11-*cis* retinol dehydrogenase, which is essential for the regeneration of visual pigment.<sup>4,5</sup> Classically, FA has been described<sup>6</sup> as stationary night blindness with delayed dark adaptation with normal visual acuity and color vision. More recent studies<sup>7-9</sup> have shown that cone dystrophy is present in some patients with FA, particularly in older individuals. Using conventional fundus autofluorescence (FAF) imaging methods, the albipunctate spots have been reported to be hyperfluorescent in some studies<sup>10,11</sup> and hypofluorescent in others.<sup>12</sup> Spectral domain optical coherence tomography has shown<sup>10-13</sup> that the spots extend from the RPE to the outer retinal layers. These methods, however, are limited by their resolution and do not provide in vivo morphologic assessment of FA at the cellular level.

Adaptive optics has enabled high-resolution retinal imaging of the cone photoreceptor mosaic in vivo,<sup>14-18</sup> providing the opportunity to characterize retinal diseases.<sup>19-22</sup> A recent report<sup>23</sup> using an adaptive optics scanning laser ophthalmoscope (AOSLO) prototype to study individuals with FA described dark patches in the cone mosaic, with decreased cone density at 0.5° and 1° from the foveal center. In the present study, we used an AOSLO to measure the cone photoreceptors from the fovea to 10° eccentricity and a fluorescence AOSLO (FAOSLO) to examine the albipunctate spots in a patient with FA.

## Methods

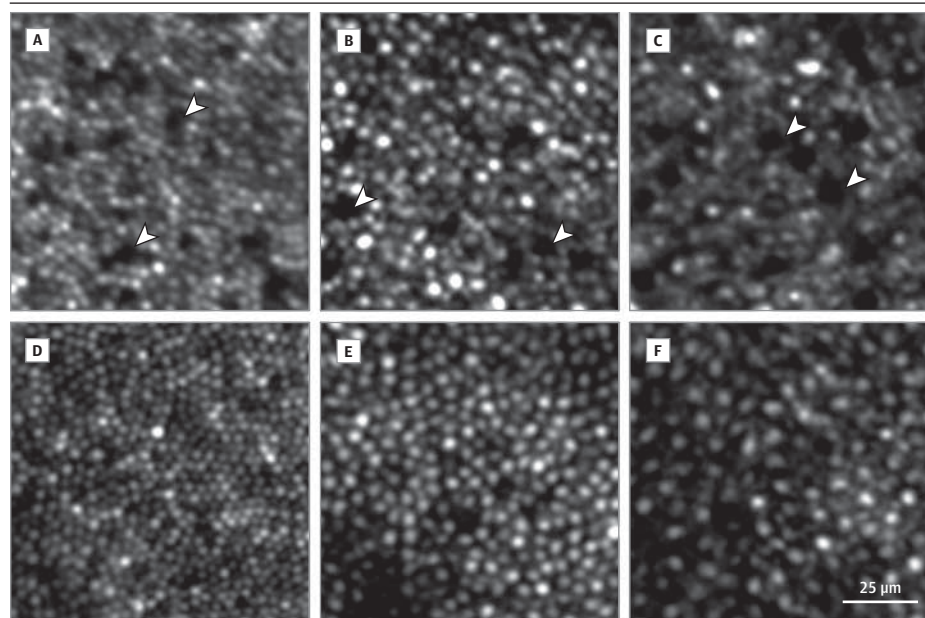
### Clinical Examination

This study was approved by the University of Rochester Research Subjects Review Board and was performed in accordance with the Declaration of Helsinki. Written informed consent was obtained and participants received financial compensation. A complete ophthalmic examination, including Snellen visual acuity measurement and dilated fundus examination, was performed. Fundus photographs (FF450 plus; Carl Zeiss Meditec), conventional FAF (HRA; Heidelberg Engineering), spectral domain optical coherence tomography (InVivoVue Envisu R2200; BiopTigen Inc), and Goldmann visual fields were obtained. Full-field electroretinography (ERG) (UTAS-E4000; LKC Technologies) was performed in accordance with the standards of the International Society for Clinical Electrophysiology of Vision.<sup>24</sup>

### Image Acquisition and Processing

Reflectance and autofluorescence images were acquired using the Rochester FAOSLO system.<sup>25,26</sup> The participant's pupils were dilated with tropicamide, 1%, and phenylephrine hydrochloride, 2.5%, and the participant's pupil remained aligned with the instrument pupil during the imaging session. The FAOSLO reflectance image sequences were obtained in approximately 1.5° × 1.5° images beginning in the central fovea, extending 10° peripherally along the superior and temporal meridians, using a fixation target to guide fixation in 0.75° steps. Two hundred images at a 19-Hz frame rate were acquired at each retinal location, and video frames were averaged after imaging.<sup>27</sup> At selected retinal locations with albipunctate spots, autofluorescence (excitation, 561 nm; emission, 624 Δ 40 nm) images were

Figure 1. Fluorescence Adaptive Optics Scanning Laser Ophthalmoscope (FAOSLO) Reflectance Images of the Cone Mosaic at Selected Eccentricities in the Temporal Retina



Patient with fundus albipunctatus (FA) (A, B, and C). Bottom row, age-matched individual with healthy eyes (D, E, and F). Images from the foveal center at 200 μm (A and D), 700 μm (B and E), and 2100 μm (C and F). White arrowheads indicate cones with decreased core reflectance (dark cones) in the patient with FA.

simultaneously acquired. Using the reflectance images as a guide, approximately 1000 autofluorescence frames were registered at each location.<sup>28</sup> Image montaging was performed using Adobe Photoshop, version 12.1 X64 (Adobe Systems).

### Determination of the Foveal Center

The location of the foveal center in the FAOSLO reflectance image was determined using a 2-step process. First, 30 locations along the retinal capillaries delineating the foveal avascular zone (FAZ) were manually selected. Using custom software (MATLAB, version 2011.b; MathWorks Inc), an ellipse was fit to these points and the center of the ellipse was localized. All cone photoreceptors within a  $290 \times 290\text{-}\mu\text{m}$  square centered at this point were marked semiautomatically.<sup>18</sup> A cone density map was generated using a  $36 \times 36\text{-}\mu\text{m}$  sliding window with  $10\text{-}\mu\text{m}$  overlap.<sup>29</sup> Cone densities were corrected using the participant's axial length compared with the Gullstrand model eye.<sup>30</sup> The point of highest cone density was then defined as the foveal center.

### Cone Labeling, Density, and Spacing Computation

Cones were analyzed along the superior and temporal meridians. Forty concentric circles at  $100\text{-}\mu\text{m}$  intervals were drawn from the foveal center to  $10^\circ$ . The distance of each circle was calculated from the Gullstrand model eye with correction for axial length. Windows of  $50 \times 50\text{-}\mu\text{m}$  were selected along each meridian at every  $100\text{-}\mu\text{m}$  referenced by these concentric circles. When blood vessels or defects in the image quality were present along the meridian, the sampling regions were slightly displaced along the concentric circle. For each sampling location, eccentricity was computed as the distance between the center of the window and the foveal center. Cone photoreceptors in these windows were labeled (*distinct cones*). Because some cones showed a decreased core reflectance (*dark cones*), we used a logarithmic grayscale transformation of the reflectance image<sup>31</sup> to enhance visualization of the dark cones, and labeled these separately. Cone spacing was calculated<sup>32</sup> for the distinct cones as well as the total of both the distinct and dark cones.

### Statistical Analysis

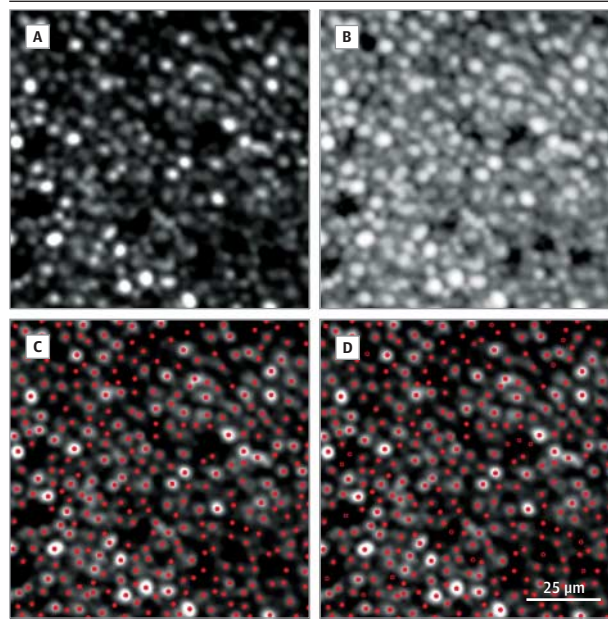
Cone density and spacing were compared with available published normative data. At the foveal center ( $<200\text{-}\mu\text{m}$  retinal eccentricity), histologic data were used.<sup>28</sup> At  $200\text{-}\mu\text{m}$  retinal eccentricity and above, AOSLO normal cone density data were used for comparison.<sup>18</sup> For the AOSLO normal cone density data, exponential fit curves were generated (mean cone density  $\pm 2$  SD). Normal cone densities as a function of eccentricity then were calculated at  $100\text{-}\mu\text{m}$  intervals. Cone densities were converted to cone spacing,<sup>32</sup> and a z score of 2 (2 SDs from the mean) was used for comparison with the patient with FA. The sign test<sup>33</sup> was applied to compare the cone spacing z scores of the patient with FA with the normative data along the superior and temporal meridians.

## Results

### Clinical Findings

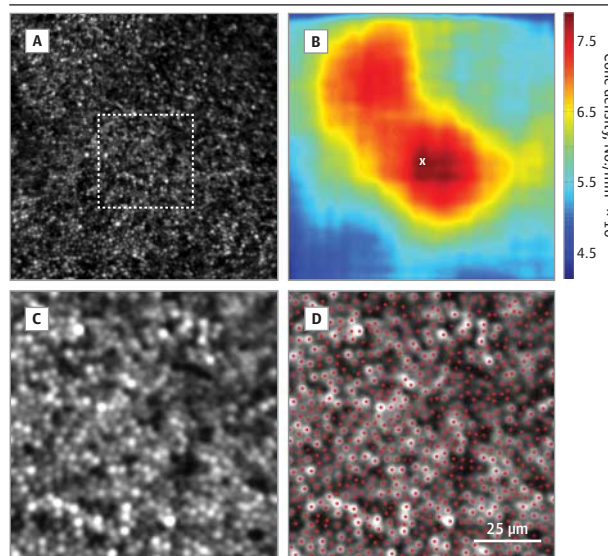
A woman in her 30s presented with progressively worsening night vision. Best-corrected visual acuity measured 20/25 + 1 OD

Figure 2. Labeling of Distinct Cones and Dark Cones



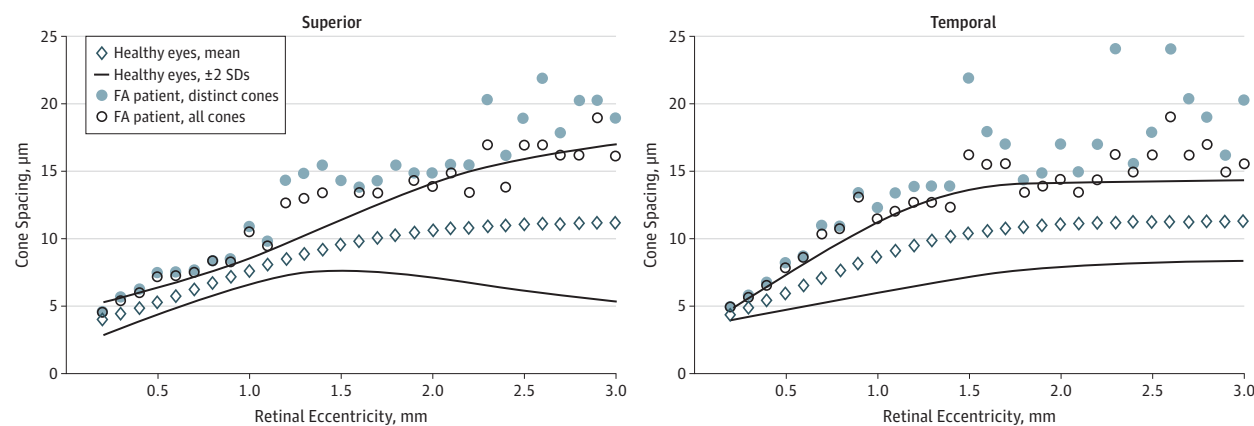
A, Fluorescence adaptive optics scanning laser ophthalmoscope (FAOSLO) reflectance image ( $700\text{-}\mu\text{m}$  temporal) shows distinct cones as well as dark cones in the patient with fundus albipunctatus. B, Logarithmic grayscale transformation of the same temporal area enables visualization of the dark cone cores. C, Cone labeling of only distinct cones. D, Cone labeling of both distinct cones (solid red circles) and dark cones (open red circles).

Figure 3. Foveal Cone Density Mapping Shows Reduced Peak Foveal Cone Density



A, Fluorescence adaptive optics scanning laser ophthalmoscope (FAOSLO) reflectance image of the cone mosaic in a  $290 \times 290\text{-}\mu\text{m}$  window centered on the center of the foveal avascular zone. The white square indicates a  $100 \times 100\text{-}\mu\text{m}$  window shown at higher magnification in panel C, centered on the location of peak cone density. B, Cone density map of the central  $290 \times 290\text{-}\mu\text{m}$  window. The color bar at the right indicates cone density in cones per squared millimeters. The location of peak cone density is marked (white x). C, Reflectance image of the central  $100 \times 100\text{-}\mu\text{m}$  window shows multiple dark cones. D, Cone labeling of distinct cones (solid red circles) and dark cones (open red circles).

Figure 4. Cone Spacing as a Function of Eccentricity



Cone spacing was significantly increased in comparison with the normal range (sign test,  $P = .045$ ). Circles indicate the cone spacing of the patient with fundus albipunctatus (FA) (open circles indicate distinct cones, and solid circles,

distinct + dark cones). Mean age-matched normal cone spacing data are indicated by diamond symbols (solid lines indicate  $\pm 2$  SD).<sup>18</sup>

and 20/20 – 2 OS. Dilated fundus examination revealed multiple radial round yellow-white spots distributed throughout the peripheral retina, characteristic of FA (Supplement [eFigure 1]).

No albipunctate spots were present in the central macula, and the foveal reflex was visualized (Supplement [eFigure 2A]). Conventional FAF images showed bright spots corresponding to the albipunctate spots; however, features of the optic nerve head were also visible in these images, suggesting light reflectance artifact (Supplement [eFigure 2B]). Spectral domain optical coherence tomography showed that the albipunctate spots extended from the RPE to the outer nuclear layer. The photoreceptor outer segment layer was slightly granular in appearance (Supplement [eFigure 2C]).

Goldmann visual fields showed slight loss of superior visual field in the I2e isopter in both eyes. Dark adapted, dim flash b-wave amplitude was reduced by approximately 25%. Photopic, bright flash, and flicker amplitudes were within normal limits.

#### Structural Appearance of Cones in Disease

The FAOSLO reflectance imaging demonstrated a continuous cone mosaic with single-cell resolution at all locations, including the foveal center. The cone structure was highly variable, with many cones having decreased core reflectance (dark cones) (Figure 1). Similar findings of decreased core reflectance have been reported<sup>34</sup> in patients with achromatopsia and may represent shortening of the cone outer segments. Logarithmic grayscale transformation enhances visualization of the dark cones to enable more accurate cone labeling in the setting of retinal disease (Figure 2).

#### Reduced Cone Packing Density and Increased Cone Spacing Measurements

Cone density mapping (Figure 3) showed that the peak foveal cone density was reduced to 70% of the lower limit of the reference range<sup>29</sup> ( $78.7 \times 10^3$  cones/mm<sup>2</sup>; mean [SD] reference range,  $199 [87] \times 10^3$  cones/mm<sup>2</sup>). Peripherally, cone spacing

was significantly increased in comparison with healthy, unaffected individuals<sup>18</sup> (sign test,  $P = .045$ ) (Figure 4).

#### High Reflectance and Hypoautofluorescence of Albipunctate Spots

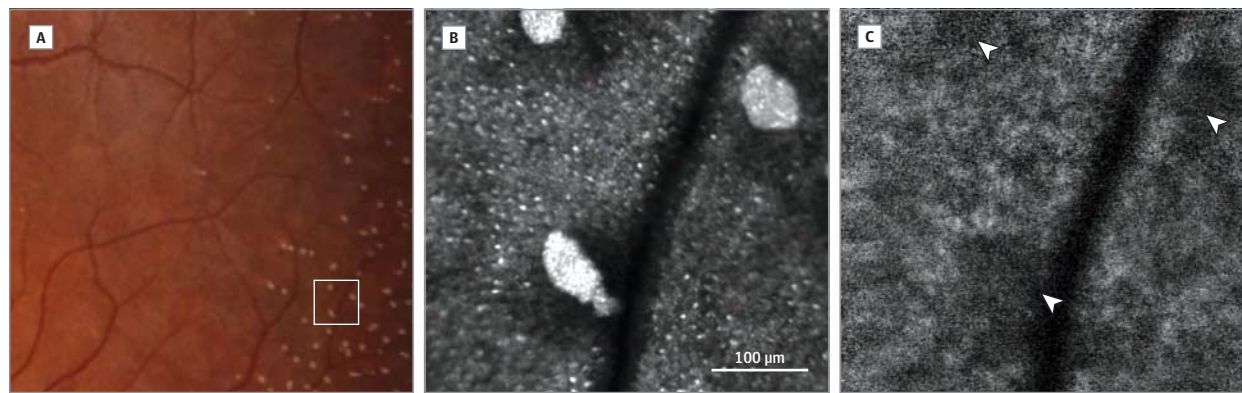
The FAOSLO reflectance imaging showed bright reflectance with no visible photoreceptors in the areas corresponding to the albipunctate spots (Figure 5B). The FAOSLO images obtained at the same locations demonstrated hypoautofluorescence corresponding to the albipunctate spots (Figure 5C). No RPE cells were discernible at these lesions, perhaps because of blockage of the autofluorescent signal.

#### Discussion

The advent of FAOSLO technology has provided novel in vivo morphologic data at the cellular level in a patient with FA. Although the clinical findings, including presenting symptoms of night blindness, excellent central visual acuity, and decreased scotopic with normal photopic ERG amplitudes, were suggestive of a primary rod dysfunction, use of the FAOSLO demonstrated a significant reduction in cone density at the foveal center and increased cone spacing peripherally extending to 10°. Although cone density at the foveal center is variable in individuals with healthy eyes,<sup>18,35</sup> the peak foveal cone density in the patient with FA described here was 30% below the lower limit of the reported reference range. This finding is consistent with a recent report<sup>23</sup> of decreased cone densities at 0.5° and 1° eccentricity in patients with FA.

The morphologic appearance of the cones was also disrupted, with many cones showing diminished reflectance of the central core. We have termed these *dark cones* and have included a method to help identify them in cone counting. Healthy cones have robust waveguiding properties, lending them the appearance of a bright central core on AOSLO reflectance imaging. Although some variability in cone reflectance

Figure 5. Fluorescence Adaptive Optics Scanning Laser Ophthalmoscope (FAOSLO) Images of the Albipunctate Spots



A, Color fundus photograph of the temporal retina. White square indicates the location shown at higher magnification in panels B and C. B, FAOSLO reflectance image of the temporal retina shows bright reflectance of the albipunctate spots. Cones are visualized between spots, but no cones are identified at the location of the spots. C, FAOSLO autofluorescence image

acquired at the same retinal location. The albipunctate spots are hypoautofluorescent (white arrows). Between spots, a honeycomb pattern indicative of the retinal pigment epithelium (RPE) cell mosaic is present. No RPE cells are discernible underlying the albipunctate spots.

occurs in individuals with healthy eyes and varies over time,<sup>36</sup> diminished cone core reflectance has been reported<sup>30</sup> in achromatopsia and may indicate shortening of the cone outer segments in retinal degenerations. The spectral domain optical coherence tomography finding of subtle granularity in the outer segment layer further substantiates this interpretation. The development of metrics to quantify the variability in cone reflectance, compared with normative data, would help to characterize this feature in retinal disease.

Conventional FAF images showed bright spots corresponding to the albipunctate spots, but FAOSLO imaging demonstrated hypoautofluorescence of the albipunctate spots. In the conventional FAF images, features within the optic disc were also visible, suggesting an artifact caused by reflected light. The Heidelberg HRA uses 488-nm excitation and collects emitted light above 500 nm. The FAOSLO system uses 561-nm excitation, with emission of 624  $\Delta$  40 nm. Both systems include the expected emission of lipofuscin autofluorescence; however, the narrower bandwidth of the filters used in the FAOSLO system are more selective for lipofuscin autofluorescence. In addition, the FAOSLO system design uses a series of 2 filters, allowing minimal light leak (<0.01%). The highly reflective albipunctate spots likely caused the light artifact in the conventional FAF images. This explanation would account for the variable results previously reported in the literature.<sup>10-12</sup> The hypoautofluorescence demonstrated by FAOSLO indicates that the albipunctate spots do not represent lipofuscin. Neither cones nor RPE cells were detected in the location of the spots. It is possible that these cells were not present in these loca-

tions because of the disease or that the highly reflective albipunctate spots precluded FAOSLO imaging of these cells. Other possible explanations include that cones were present but altered in their waveguiding or packing properties so that they were not detectable by FAOSLO examination, or that the cells were outside the plane of focus owing to the presence of the albipunctate lesions.

It is tempting to hypothesize that the decreased cone density revealed by FAOSLO in this young patient with normal photopic ERG represents an early sign of progression to a macular phenotype that could worsen with aging. Phenotypic diversity has been reported,<sup>11</sup> with cone dystrophy notably present among older affected individuals. Longitudinal follow-up of the patient described here and other patients will be necessary to determine whether cone dystrophy represents a late stage of progressive FA disease.

## Conclusions

Although conventional methods suggest a primary rod dysfunction in fundus albipunctatus, examination using FAOSLO revealed a significant reduction in cone density at the foveal center and increased cone spacing peripherally. Dark cones were present, suggesting loss of photoreceptor outer segments. The albipunctate spots were hypoautofluorescent and likely do not represent lipofuscin. With these results, FAOSLO can provide a method to detect early signs of the macular phenotype in FA.

### ARTICLE INFORMATION

**Submitted for Publication:** November 22, 2013; final revision received February 13, 2014; accepted February 20, 2014.

**Published Online:** June 12, 2014.  
doi:10.1001/jamaophthalmol.2014.1079.

**Author Contributions:** Dr Chung had full access to all the data in the study and takes responsibility for

the integrity of the data and the accuracy of the data analysis.

**Study concept and design:** All authors.

**Acquisition, analysis, or interpretation of data:** All authors.

**Drafting of the manuscript:** All authors.

**Critical revision of the manuscript for important intellectual content:** All authors.

**Statistical analysis:** Song, Williams.

**Obtained funding:** Williams, Chung.

**Administrative, technical, or material support:** Song, Latchney, Williams.

**Study supervision:** All authors.

**Conflict of Interest Disclosures:** Dr Song is collaborating with Canon, Inc on a research contract funded by Canon to help them commercialize the technology described in this report. Dr Williams is

an inventor and receives royalties from licensed patents held by the University of Rochester pertaining to the adaptive optics imaging technology used in this study and is collaborating with Canon, Inc on a research contract funded by Canon to help them commercialize this technology. Dr Chung is a consultant for GlaxoSmithKline and is currently collaborating with Canon, Inc on a research contract funded by Canon to help them commercialize this technology.

**Funding/Support:** This work was supported in part by National Institutes of Health grants EY021786, EY014375, and EY001319; the Edward N. and Della L. Thome Memorial Foundation; the University of Rochester Clinical Trials and Science Institute award number UL1 RRO24160 from the National Center for Research Resources and the National Center for Advancing Translational Sciences of the National Institutes of Health; and an unrestricted departmental grant from Research to Prevent Blindness.

**Role of the Sponsor:** The sponsors had no role in the design and conduct of the study; collection, management, analysis, and interpretation of the data; preparation, review, or approval of the manuscript; and decision to submit the manuscript for publication.

**Additional Contributions:** Jennifer Hunter, PhD (Flaum Eye Institute and Center for Visual Science, University of Rochester), assisted with statistical analysis and Margaret Folwell, MS (Center for Visual Science, University of Rochester), assisted with image processing. The contributors did not receive financial compensation.

## REFERENCES

- Dryja TP. Molecular genetics of Oguchi disease, fundus albipunctatus, and other forms of stationary night blindness: LVII Edward Jackson Memorial Lecture. *Am J Ophthalmol*. 2000;130(5):547-563.
- Yamamoto H, Simon A, Eriksson U, Harris E, Berson EL, Dryja TP. Mutations in the gene encoding 11-cis retinol dehydrogenase cause delayed dark adaptation and fundus albipunctatus. *Nat Genet*. 1999;22(2):188-191.
- Gonzalez-Fernandez F, Kurz D, Bao Y, et al. 11-Cis retinol dehydrogenase mutations as a major cause of the congenital night-blindness disorder known as fundus albipunctatus. *Mol Vis*. 1999;5:41. <http://www.molvis.org/molvis/v5/p41/>. Published December 30, 1999. Accessed September 20, 2013.
- Driessen CAGG, Winkens HJ, Hoffmann K, et al. Disruption of the 11-cis-retinol dehydrogenase gene leads to accumulation of cis-retinols and cis-retinyl esters. *Mol Cell Biol*. 2000;20(12):4275-4287.
- Farjo KM, Moiseyev G, Takahashi Y, Crouch RK, Ma JX. The 11-cis-retinol dehydrogenase activity of RDH10 and its interaction with visual cycle proteins. *Invest Ophthalmol Vis Sci*. 2009;50(11):5089-5097.
- Heckenlively JR, Martin DA, Rosenbaum AL. Loss of electroretinographic oscillatory potentials, optic atrophy, and dysplasia in congenital stationary night blindness. *Am J Ophthalmol*. 1983;96(4):526-534.
- Miyake Y, Shirogama N, Sugita S, Horiguchi M, Yagasaki K. Fundus albipunctatus associated with cone dystrophy. *Br J Ophthalmol*. 1992;76(6):375-379.
- Nakamura M, Hotta Y, Tanikawa A, Terasaki H, Miyake Y. A high association with cone dystrophy in fundus albipunctatus caused by mutations of the RDH5 gene. *Invest Ophthalmol Vis Sci*. 2000;41(12):3925-3932.
- Niwa Y, Kondo M, Ueno S, Nakamura M, Terasaki H, Miyake Y. Cone and rod dysfunction in fundus albipunctatus with RDH5 mutation: an electrophysiological study. *Invest Ophthalmol Vis Sci*. 2005;46(4):1480-1485.
- Genead MA, Fishman GA, Lindeman M. Spectral-domain optical coherence tomography and fundus autofluorescence characteristics in patients with fundus albipunctatus and retinitis punctata albescens. *Ophthalmic Genet*. 2010;31(2):66-72.
- Sergouniotis PI, Sohn EH, Li Z, et al. Phenotypic variability in RDH5 retinopathy (fundus albipunctatus). *Ophthalmology*. 2011;118(8):1661-1670.
- Schatz P, Preising M, Lorenz B, et al. Lack of autofluorescence in fundus albipunctatus associated with mutations in RDH5. *Retina*. 2010;30(10):1704-1713.
- Querques G, Carrillo P, Querques L, Bux AV, Del Curatolo MV, Delle Noci N. High-definition optical coherence tomographic visualization of photoreceptor layer and retinal flecks in fundus albipunctatus associated with cone dystrophy. *Arch Ophthalmol*. 2009;127(5):703-706.
- Liang J, Williams DR, Miller DT. Supernormal vision and high-resolution retinal imaging through adaptive optics. *J Opt Soc Am A Opt Image Sci Vis*. 1997;14(11):2884-2892.
- Roorda A, Romero-Borja F, Donnelly Iii W, Queener H, Hebert T, Campbell M. Adaptive optics scanning laser ophthalmoscopy. *Opt Express*. 2002;10(9):405-412.
- Chui TYP, Song H, Burns SA. Individual variations in human cone photoreceptor packing density: variations with refractive error. *Invest Ophthalmol Vis Sci*. 2008;49(10):4679-4687.
- Chui TYP, Song HX, Burns SA. Adaptive-optics imaging of human cone photoreceptor distribution. *J Opt Soc Am A Opt Image Sci Vis*. 2008;25:3021-3029.
- Song H, Chui TY, Zhong Z, Elsner AE, Burns SA. Variation of cone photoreceptor packing density with retinal eccentricity and age. *Invest Ophthalmol Vis Sci*. 2011;52(10):7376-7384.
- Wolfing JI, Chung M, Carroll J, Roorda A, Williams DR. High-resolution retinal imaging of cone-rod dystrophy. *Ophthalmology*. 2006;113(6):1014-1019.e1. doi:10.1016/j.ophtha.2006.01.056.
- Roorda A, Zhang Y, Duncan JL. High-resolution in vivo imaging of the RPE mosaic in eyes with retinal disease. *Invest Ophthalmol Vis Sci*. 2007;48(5):2297-2303.
- Duncan JL, Zhang Y, Gandhi J, et al. High-resolution imaging with adaptive optics in patients with inherited retinal degeneration. *Invest Ophthalmol Vis Sci*. 2007;48(7):3283-3291.
- Kim JE, Chung M. Adaptive optics for retinal imaging: current status. *Retina*. 2013;33(8):1483-1486.
- Makiyama Y, Ooto S, Hangai M, et al. Cone abnormalities in fundus albipunctatus associated with RDH5 mutations assessed using adaptive optics scanning laser ophthalmoscopy. *Am J Ophthalmol*. 2014;157(3):558-570.e1-4. doi:10.1016/j.ajo.2013.10.021.
- Marmor MF, Fulton AB, Holder GE, Miyake Y, Brigell M, Bach M; International Society for Clinical Electrophysiology of Vision. ISCEV Standard for full-field clinical electroretinography (2008 update). *Doc Ophthalmol*. 2009;118(1):69-77.
- Dubra A, Sulai Y. Reflective afocal broadband adaptive optics scanning ophthalmoscope. *Biomed Opt Express*. 2011;2(6):1757-1768.
- Gray DC, Merigan W, Wolfing JI, et al. In vivo fluorescence imaging of primate retinal ganglion cells and retinal pigment epithelial cells. *Opt Express*. 2006;14(16):7144-7158.
- Dubra A, Harvey Z. Registration of 2D images from fast scanning ophthalmic instruments. In: Fischer B, Dawant B, Lorenz C, eds. *Biomedical Image Registration*. Berlin, Germany: Springer; 2010:60-71.
- Morgan JI, Dubra A, Wolfe R, Merigan WH, Williams DR. In vivo autofluorescence imaging of the human and macaque retinal pigment epithelial cell mosaic. *Invest Ophthalmol Vis Sci*. 2009;50(3):1350-1359.
- Curcio CA, Sloan KR, Kalina RE, Hendrickson AE. Human photoreceptor topography. *J Comp Neurol*. 1990;292(4):497-523.
- de Almeida MS, Carvalho LA. Different schematic eyes and their accuracy to the in vivo eye: a quantitative comparison study. *Braz J Phys*. 2007;37:378-387.
- Dubra A, Sulai Y, Norris JL, et al. Noninvasive imaging of the human rod photoreceptor mosaic using a confocal adaptive optics scanning ophthalmoscope. *Biomed Opt Express*. 2011;2(7):1864-1876.
- Rossi EA, Roorda A. The relationship between visual resolution and cone spacing in the human fovea. *Nat Neurosci*. 2010;13(2):156-157.
- Dixon WJ, Mood AM. The statistical sign test. *J Am Stat Assoc*. 1946;41(236):557-566.
- Genead MA, Fishman GA, Rha J, et al. Photoreceptor structure and function in patients with congenital achromatopsia. *Invest Ophthalmol Vis Sci*. 2011;52(10):7298-7308.
- Dees EW, Dubra A, Baras RC. Variability in parafoveal cone mosaic in normal trichromatic individuals. *Biomed Opt Express*. 2011;2(5):1351-1358.
- Pallikaris A, Williams DR, Hofer H. The reflectance of single cones in the living human eye. *Invest Ophthalmol Vis Sci*. 2003;44(10):4580-4592.